Cost-effective clean ammonia production using membrane-assisted autothermal reforming

Schalk Cloete[a,*], Mohammed Nazeer Khan[b,c], Shareq Mohd Nazir[b,d], Shahriar Amini[a,e]

[a] *SINTEF Industry, Trondheim, Norway*
[b] *Norwegian University of Science and Technology, Trondheim, Norway*
[c] *Flemish Institute for Technological Research (VITO), Mol, Belgium*
[d] *KTH Royal Institute of Technology, Stockholm, Sweden*
[e] *Department of Mechanical Engineering, University of Alabama, Tuscaloosa, USA*

HIGHLIGHTS

- Membrane-assisted autothermal reforming (MA-ATR) produces clean hydrogen.
- MA-ATR is synergistically integrated into an ammonia plant with 100% CO_2 capture.
- The integration greatly simplifies the plant layout and increases efficiency by 10.7%
- Costs are reduced by 14.9% relative to a reference ammonia plant with CO_2 capture.

ARTICLE INFO

ABSTRACT

Ammonia is a widely produced industrial chemical, primarily for use in the fertilizer industry. Recently, interest has also grown in ammonia as a carbon-free energy carrier because it is easier to store and transport than hydrogen. However, ammonia is primarily produced from natural gas with a considerable carbon footprint if the produced CO_2 is not captured and stored. This work therefore presents a new ammonia production method based on membrane-assisted autothermal reforming (MA-ATR) for hydrogen production from natural gas with integrated CO_2 capture. The MA-ATR reactor offers great process intensification benefits, leading to considerable efficiency gains as well as a simpler and cheaper plant. In the base case, MA-ATR achieves 10.7% greater efficiency, 14.9% lower NH_3 production costs and 16.5%-points greater CO_2 avoidance than a conventional ammonia plant where captured CO_2 is compressed for transport and storage. This economic advantage of MA-ATR increases with higher natural gas prices, lower electricity prices, lower membrane costs and higher CO_2 prices. All elements of the proposed plant are mature technologies aside from the membranes and the oxygen carrier material. Further development and demonstration of these two elements is therefore recommended to realize the promising techno-economic performance reported in this study.

1. Introduction

There is an increasing sense of urgency about the need to reduce global greenhouse gas emissions in line with a 1.5–2 °C temperature rise by the end of 21st century. Meeting this goal will require deep decarbonization of all sectors of the economy [1]. This includes not only electricity production, where many options are available, but also industry, transport and heat, where the number of viable options is more limited.

Momentum has once again been gathering behind clean hydrogen

as a viable solution to such a global deep decarbonization effort [2]. Not only can hydrogen fuel technically displace most emissions from the challenging sectors mentioned above, but it can also serve as a form of energy storage to facilitate the integration of more variable renewable energy (wind and solar). However, relative to conventional fossil fuels, the low energy density of hydrogen makes it expensive to store and distribute. Ammonia has been identified as one of the potential ways to overcome these challenges facing hydrogen fuel. Currently, 45% [2] of pure hydrogen production from natural gas is used in ammonia synthesis that forms the main element in nitrogen-based

* Corresponding author at: S.P. Andersens vei 15B, 7031 Trondheim, Norway.
E-mail address: schalk.cloete@sintef.no (S. Cloete).

List of symbols

Acronyms

ASU	Air separation unit
ATR	Autothermal reforming
CCS	CO_2 capture and storage
CLR	Chemical looping reforming
FTR	Fired tubular reformer
GSR	Gas switching reforming
LHV	Lower heating value
LNG	Liquified natural gas
MA-ATR	Membrane-assisted autothermal reforming
MA-CLR	Membrane-assisted chemical looping reforming
MDEA	Methyl diethanolamine
PSA	Pressure swing adsorption
S/U	Storage or utilization
WGS	Water-gas shift

Symbols

ϵ	Energy intensity (GJ/ton)
η	Efficiency (fraction)
C	Annualized cost (€/year)
c	Cost (€)
CAC	CO_2 avoidance costs (€/ton)
d	Discount rate (%)
E	CO_2 emissions intensity (ton/GJ)
e	Specific CO_2 emissions intensity (ton_{CO2}/ton_{NH3})
l	Economic lifetime (years)
LC	Levelized cost (€/ton)
LHV	Lower heating value (MJ/kg)
$\dot{m}$	Mass flow rate (kg/s)
$\dot{W}$	Power (MW)

Subscripts

el	Electricity
eq	Equivalent
NG	Natural gas
NH_3	Ammonia

fertilizers. Ammonia can also be combusted in internal combustion engines, gas turbines and boilers to fuel a wide range of transport and power applications, or converted back to hydrogen at the point of use for fuelling hydrogen fuel cells [2]. The Haber-Bosch process for producing ammonia from a 3:1 mixture of hydrogen and nitrogen has been in commercial operation for decades. Hence, cost reduction potential for ammonia production is limited to reducing the feedstock cost (mainly hydrogen). Low-cost clean hydrogen production is therefore essential for producing economically viable clean ammonia.

The recent special report on hydrogen from the International Energy Agency [2] contains a comparative assessment of different hydrogen production pathways, projecting that electrolysis from renewable electricity will only be competitive with natural gas reforming with CO_2 capture in regions with excellent wind and solar resources that rely on natural gas imports. Furthermore, this assessment does not consider the possibility of advanced reforming pathways to produce clean hydrogen at or even below the costs of conventional steam methane reforming (SMR) without CO_2 capture.

A class of technologies capable of such cost-effective CO_2 capture is chemical looping reforming (CLR) [3,4], originally derived from chemical looping combustion [5,6]. In CLR, an oxygen carrier material that also acts as a reforming catalyst (generally NiO) is circulated between two reactors. In the air reactor, the oxygen carrier is oxidized with air, producing a hot N_2-rich outlet stream. The oxidized oxygen carrier is then transported to the fuel reactor where it oxidizes and reforms a hydrocarbon fuel to syngas that is not diluted with any N_2 from air. In this case, the oxygen carrier also transports heat from the highly exothermic oxidation reaction in the air reactor to the endothermic reforming reaction in the fuel reactor.

For pure hydrogen production, this configuration can be applied in a gas switching reforming (GSR) [7,8] concept where the fuel oxidation and reforming in the fuel reactor of CLR is inherently split into two separate steps. This allows for the natural integration of a pressure swing adsorption (PSA) unit for pure hydrogen production because the PSA off-gas can be fed to the GSR reactor to reduce the oxygen carrier and produce a pure CO_2 stream before a mix of methane and steam is fed for reforming. The GSR concept can produce hydrogen at CO_2 avoidance costs as low as $15/ton [9]. A similar configuration was also recently investigated using packed bed CLR, resulting in higher CO_2 avoidance costs of $60/ton [10], largely due to a lower degree of heat integration.

Another configuration relying on the chemical looping principle for hydrogen production is a three-reactor configuration [11] relying on the steam-iron reaction [12]. This process was assessed to produce clean hydrogen with a CO_2 avoidance cost of €19.5/ton [13]. An important scale-up challenge with this process is the need for operating three interconnected reactors at high temperature and pressure. In addition, two of the reactors must be operated as moving beds due to the equilibrium constraints of this system, introducing further challenges relating to oxygen carrier, reactor operation and reactor size.

Arguably the most fundamentally attractive hydrogen production technology based on the CLR concept is membrane-assisted chemical looping reforming (MA-CLR) [14,15]. This concept employs hydrogen perm-selective membranes in the CLR fuel reactor to extract hydrogen as it is being produced via reforming. Fuel that is not extracted as hydrogen slips past the membranes where it reacts with oxidized oxygen carrier entering the fuel reactor from the top. Due to the process intensification benefits of membranes, MA-CLR could produce H_2 with CO_2 capture at a cost that is fully 11% lower than the benchmark SMR process without CO_2 capture and 32% below the cost of SMR with post-combustion CO_2 capture [14]. Such a large cost reduction would strongly increase the feasibility of clean hydrogen for deep decarbonization of the global economy.

A potential challenge with MA-CLR is the scale-up and operation of the interconnected CLR reactor system at the high pressures required for high process efficiency. The concept requires two fluidized bed reactors in addition to cyclones, loop-seals and solids transport lines, all operating at pressures around 50 bar and temperatures up to 900 ˚C. Oxygen carrier circulation must be well controlled to supply oxygen and heat to the fuel reactor and ensure that oxidized oxygen carrier entering at the top of the fuel reactor is evenly distributed to convert all the fuel slipping past the membranes.

To simplify this challenge, the membrane-assisted autothermal reforming (MA-ATR) concept was recently proposed [16]. As illustrated in Fig. 1, MA-ATR replaces the MA-CLR air reactor and all the equipment in the solids circulation loop with a conventional cryogenic air separation unit (ASU). Hence, the oxygen carrier remains in a single autothermal bubbling fluidized bed reactor operating at steady state, greatly simplifying design, operation and scale-up relative to MA-CLR. Oxygen from the ASU is evenly injected above the membranes via a ring sparger where it oxidizes the oxygen carrier to ensure that all fuel slipping past the membranes is efficiently combusted with the
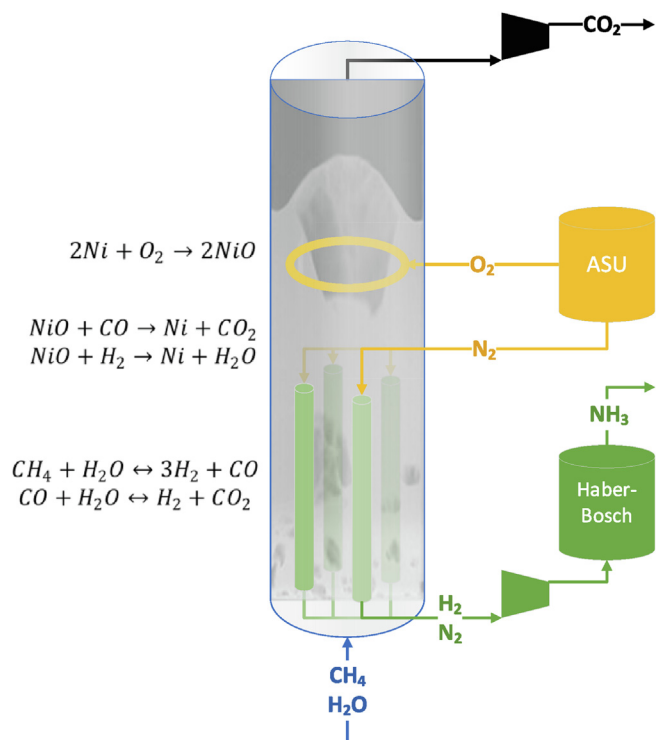
Fig. 1. Simplified schematic of the MA-ATR reactor for producing a high purity H_2 and N_2 stream for NH_3 production with integrated CO_2 capture. Reactions taking place in the different reactor regions are also shown.

stoichiometric amount of oxygen. Such oxygen carrier-mediated fuel combustion maximizes efficiency and CO_2 purity by avoiding the need for excess oxygen as required by conventional oxy-combustion. Indirect fuel combustion via the oxygen carrier also avoids any flames forming in the reactor and ensures that all the combustion heat is directly stored in the oxygen carrier with only a mild temperature rise due to its high heat capacity. This heat is then carried down to the membranes by the

oxygen carrier, which also serves as a catalyst for the reforming reactions. The energy penalty of the ASU is largely cancelled out by not having to compress a sizable quantity of N_2 to very high pressures for feeding the air reactor of the MA-CLR concept. As a result, this simplified reactor concept returned similar H_2 production costs to the MA-CLR benchmark [16], while avoiding the operational challenges associated with circulating an oxygen carrier between different reactors.

However, even if hydrogen could be produced at the low costs promised by these advanced reforming technologies, substantial techno-economic challenges remain in the distribution and storage of the produced hydrogen. For international trade and long-term storage, hydrogen storage mechanisms like ammonia [17] or liquid organic hydrogen carriers [18] will be required.

Almost all ammonia today is produced via the Haber-Bosch process using natural gas as feedstock. Such a plant has many process units and requires extensive heat integration for high efficiency, but it remains the most economical ammonia production pathway available. In an attempt to simplify the ammonia production pathway and reduce costs and emissions, several other pathways for ammonia production are currently under investigation, including several electrochemical process routes [19] and new pathways such as non-thermal plasma [20]. The Ca-Cu process has also been recently proposed for efficient ammonia production with CO_2 capture, showing promising process efficiencies [21]. Another low-carbon ammonia production pathway is biomass gasification, although a high ammonia price is needed for this option to be economically attractive [22].

The present study will investigate the potential of a novel ammonia production route based on the MA-ATR technology to create a simpler and more cost-effective pathway for ammonia production. MA-ATR offers two natural integration opportunities in an ammonia plant. First, the ASU can be configured to produce a high purity N_2 stream for combination with the pure H_2 extracted via the membranes to feed the Haber-Bosch process. Second, this N_2 stream can be fed through the membranes as a sweep gas to reduce the partial pressure of hydrogen on the permeate side, thus allowing for higher pressures in the membranes (reducing compression work required before the ammonia synthesis loop). This is illustrated in Fig. 1.

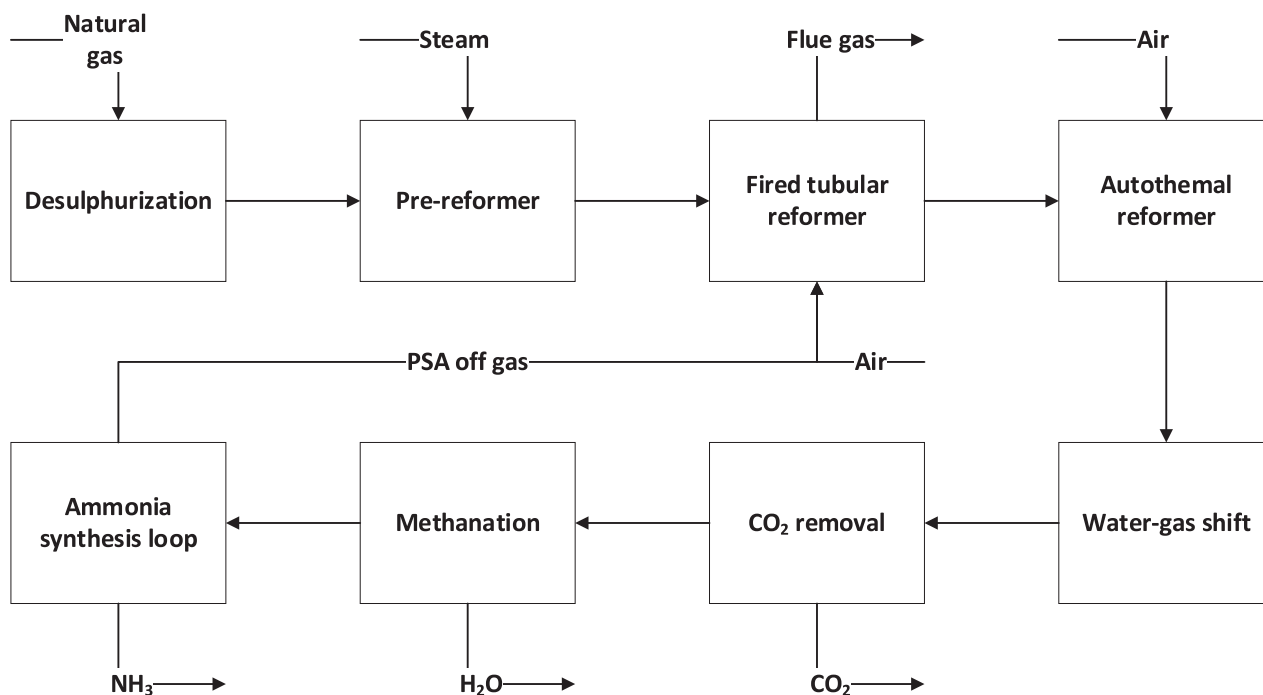In addition, the MA-ATR process can greatly simplify an ammonia

Fig. 2. Simplified process flow diagram of the benchmark ammonia production plant.

production facility. This is illustrated in the simplified block flow diagrams in Fig. 2 and Fig. 3. The MA-ATR reactor and the ASU replace the functionality of the fired tubular reformer (FTR), the autothermal reformer (ATR), the water–gas shift (WGS) reactors, the CO_2 removal unit and the methanation unit. Heat integration in the MA-ATR plant will also be substantially simpler due to the smaller number of process units, the absence of process units running exothermic reactions (WGS and methanation), much lower reformer temperatures, and avoidance of air heating in an FTR furnace. Furthermore, the ammonia synthesis loop in the MA-ATR process can be simplified substantially because of the high purity of the H_2 and N_2 mixture, which does not require a refrigeration loop to remove impurities.

The techno-economic benefits of these fundamental advantages will be quantified in the present study by comparing the MA-ATR plant to a reference ammonia production plant with and without CO_2 capture. A detailed techno-economic assessment is conducted for all three plants to harmonize the assumptions used in this comparative analysis. The sensitivity of levelized ammonia production costs to changes in important assumptions like natural gas, electricity, membrane and CO_2 prices will also be presented to quantify the robustness of the results. Prospects for enabling ammonia as a clean energy carrier of the future are also briefly discussed. Based on all this information, reliable conclusions can be drawn regarding the attractiveness of further demonstration and scale-up of the MA-ATR process for clean ammonia production.

2. Methodology

The following three sections present the methodology used in the modelling of the MA-ATR reactor, the reference and MA-ATR ammonia plants, and the economic assessment.

2.1. Reactor modelling

The MA-ATR reactor (Fig. 1) was modelled in ANSYS Fluent almost identically to the methodology reported in the previous work of the authors where the MA-ATR concept was presented for hydrogen production [16]. This model includes reaction rate expressions for the reforming [23,24] and oxygen carrier redox [25] reactions, permeation of hydrogen through the membranes [26], axial dispersion of solids species and heat [27], as well as additional modelling to account for momentum [28] and mass [29] transfer limitations caused by the mesoscale structures (bubbles) formed in the fluidized bed reactor. The equation system is outlined in the appendix of Wassie et al. [30] for more details.

One key addition to this model is required for the present work. Since the N_2 stream from the ASU is now used to sweep the membranes, species transport must also be solved within the membranes themselves. For this reason, and additional 1D domain for the membranes was set up next to the 1D domain of the reactor with mass and heat transfer between the two domains. Mass transfer was simulated according to the membrane permeation law presented by Fernandez et al. [26], while heat transfer was simulated with a heat transfer coefficient of 300 $W/m^2/K$, which is a reasonable average for tubes immersed in a fluidized bed [31].

The flow through the membranes is introduced counter-current to the flow through the reactor to ensure maximum hydrogen recovery. In other words, the N_2 sweep stream was introduced from the top of the domain, while the fuel and steam were introduced from the bottom. High purity O_2 from the ASU is injected into the bed above the membranes to create a zone of oxidized oxygen carrier that combusts any fuel gases that slip past the membranes. Other important assumptions used in the reactor model are summarized in Table 1.

Output from the reactor model is shown in Fig. 4. In the lower reactor regions, CH_4 and H_2O are continuously being converted to CO, CO_2 and H_2, with the H_2 being extracted by the membranes. The result is a gradual reduction in CH_4, H_2O and H_2 mole fraction and a rise in CO and CO_2 mole fraction. Above the membranes (reactor height greater than 5 m), the remaining CH_4, H_2 and CO reacts with the NiO oxygen carrier to form CO_2 and H_2O. The spike of O_2 injected at a height of 5.9 m to oxidize the oxygen carrier is also clearly visible.

The temperature gradually increases along the reactor height because of endothermic reforming reactions taking place in the lower regions and the exothermic oxidation reaction in the upper regions. The finite rate of axial heat dispersion implemented in the reactor model causes this axial temperature gradient.
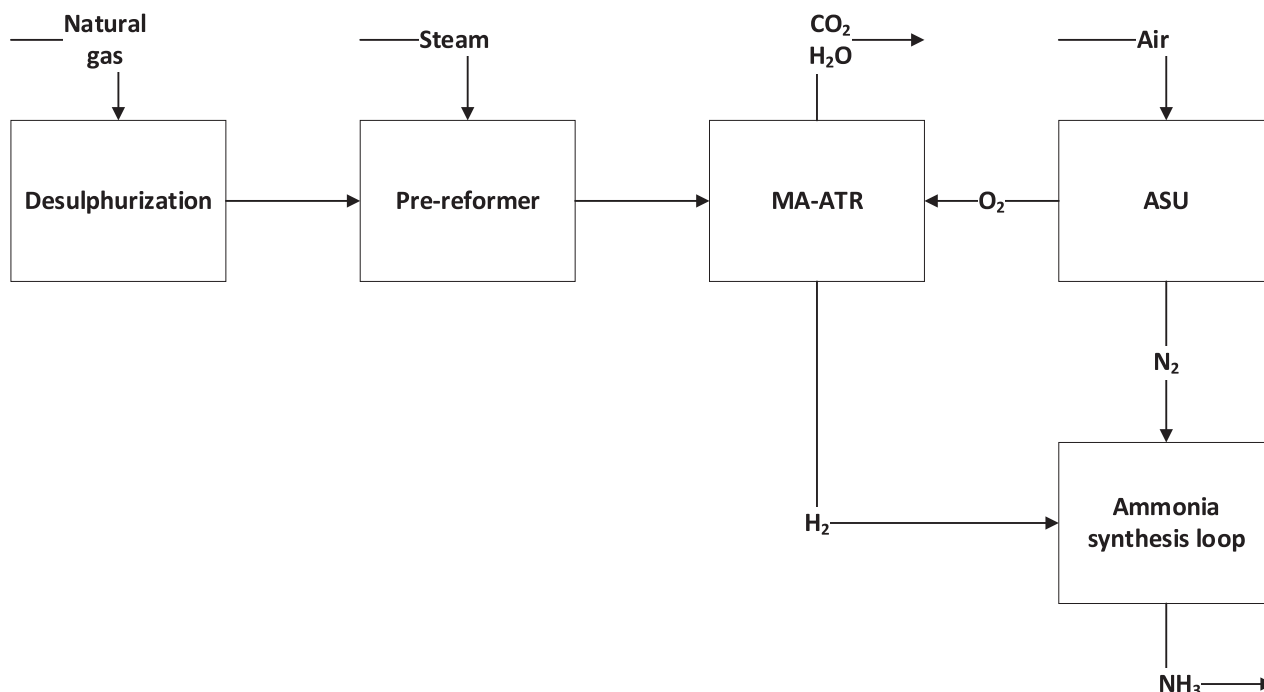

Fig. 3. Simplified process flow diagram of the proposed MA-ATR ammonia production plant.

Table 1
Assumptions in the 1D reactor modelling.

Reactor aspect ratio	2
Membrane height	Lower 60% of the reactor
Membrane volume fraction	0.5
Membrane diameter	0.05 m
Minimum P_{H_2} difference over membrane	0.2 bar
Oxygen carrier density	3400 kg/m^3
Oxygen carrier particle size	150 μm
Oxygen carrier heat capacity	1200 J/kg.K
Oxygen injection point	At 70% of the reactor height
Reactor pressure	50 bar
Membrane pressure	5 bar

Fig. 4 also shows the considerable driving force for H_2 permeation across the membranes. At all heights of the membranes (lower 5 m of the reactor) there is at least a 4 bar H_2 partial pressure difference across the membrane to drive H_2 permeation. The counter-current arrangement of the reactor ensures that the employed membrane surface area is used efficiently.

The reactor modelling was used to determine the minimum reactor size and membrane surface area that is able to extract the required amount of hydrogen. This was done by adjusting the reactor height until just enough hydrogen is extracted so that the remaining fuel gases are just enough to react with the oxygen carrier oxidized by the injected oxygen (the oxygen flowrate is determined by an energy balance over the reactor to maintain a 700 °C operating temperature). If the reactor height is too low, more fuel slips past the membranes than can be combusted by the fixed oxygen feed rate, leading to fuel slip out of the reactor. If the reactor height is too large, the reactor works well, but the
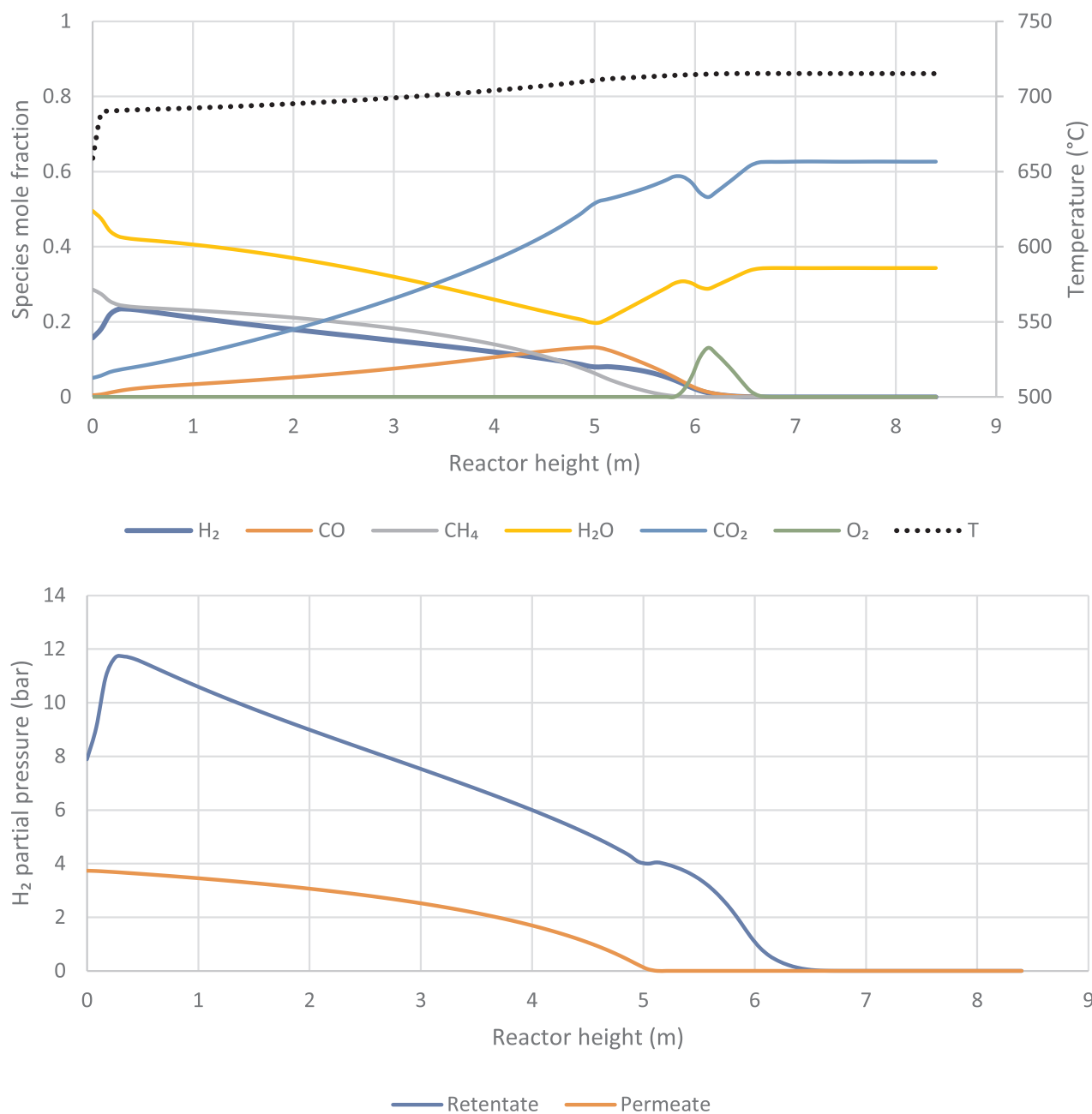

Fig. 4. Top: Simulated species and temperature profiles along the height of the MA-ATR reactor. Bottom: Simulated H_2 partial pressure inside (permeate) and outside (retentate) the membranes.

upper part of the membranes is not used efficiently because NiO diffuses downwards and reacts with the H$_2$ in the membrane region, reducing the driving force for H$_2$ permeation in the upper part of the membranes. For this study, the optimal reactor height was found to be 8.4 m (with a diameter of 4.2 m). This reactor size will therefore be used in the economic assessment.

2.2. Process modelling

The reference ammonia pant was modelled using Aspen HYSYS V8.6 [32] and the MA-ATR plant using Aspen Plus V10. Aspen HYSYS has Acid Gas thermodynamic model that is suited to simulate the absorption based CO$_2$ capture system with activated methyl diethanolamine (a-MDEA). Redlich-Kwong-Soave (RKS) equation of state with Boston-Mathias alpha function (RKS-BM) [21] is used to estimate the properties of the mixtures at equilibrium in the process, except for the CO$_2$ capture section. The pre-reformer, FTR and ATR were modelled using Gibbs Reactor module that works on the concept of minimization of the Gibbs free energy. The high temperature (HTS) and low temperature (LTS) water–gas shift reactors were modelled using the equilibrium reactor module by specifying the water–gas shift reaction. The remaining assumptions (pressure drops, compressor and turbine efficiencies etc.) to simulate the process were considered from Nazir et al. [8].

The MA-ATR process was also simulated using the RKS-BM thermodynamic model. A simple 0D mass and energy balance model was used to simulate the MA-ATR reactor [16] with the 1D model presented in the previous section used only for reactor sizing in the economic assessment. The desulphurization and pre-reformer were modelled as Gibbs reactors and the ASU was simulated directly as detailed in a previous work from the authors [16].

2.2.1. Reference plant

A state of the art ammonia plant described by Martinez et al. [21] is used as the reference in the present study. The reference plant was reproduced to maintain consistency in modeling assumptions (from [8]) and provide detailed input of different plant components to the economic assessment. Achieved efficiencies were within 2% of the values reported in Martinez et al. [21].

The schematic of the reference ammonia plant is shown in Fig. 5 with data from selected streams given in Table 2. The natural gas and steam flow to the reforming section is the same as considered in Martinez et al. [21], which is 37.80 and 96.12 ton/h respectively. Natural gas from the supply line is preheated to 369 °C and treated for sulfur removal. The desulphurized fuel is mixed with superheated steam (34.4 bar and 345 °C), pre-heated to 490 °C before being pre-reformed (in the presence of a Ni-based catalyst) to convert the higher hydrocarbons into methane. The pre-reformer outlet stream, having a steam/carbon (S/C) ratio of 2.84, is pre-heated to 620 °C and sent to a primary reformer: an FTR unit containing packed beds with reforming catalyst in a furnace that provides heat for endothermic reforming reactions and maintains the reactor temperature at 800 °C. NG and PSA off-gas fuel are combusted with air in the burners of the FTR. 59.4% of the CH$_4$ is converted to syngas in the FTR. The syngas from the FTR is further reformed with air over a reforming catalyst in the auto-thermal reformer (ATR). The air used in the ATR also provides N$_2$ for the ammonia synthesis step that needs H$_2$ and N$_2$ in a 3:1 ratio.

The synthesis gas from the ATR is cooled and sent to two water–gas shift reactors in series, one at high temperature (350 °C) and the second at low temperature (200 °C), that converts the CO and H$_2$O in the stream to H$_2$ and CO$_2$. The synthesis gas stream from the low temperature shift is cooled to 35 °C before the CO$_2$ separation section. Nearly 99% CO$_2$ from the syngas stream is then separated using a piperazine activated MDEA solution in an absorption column. The choice
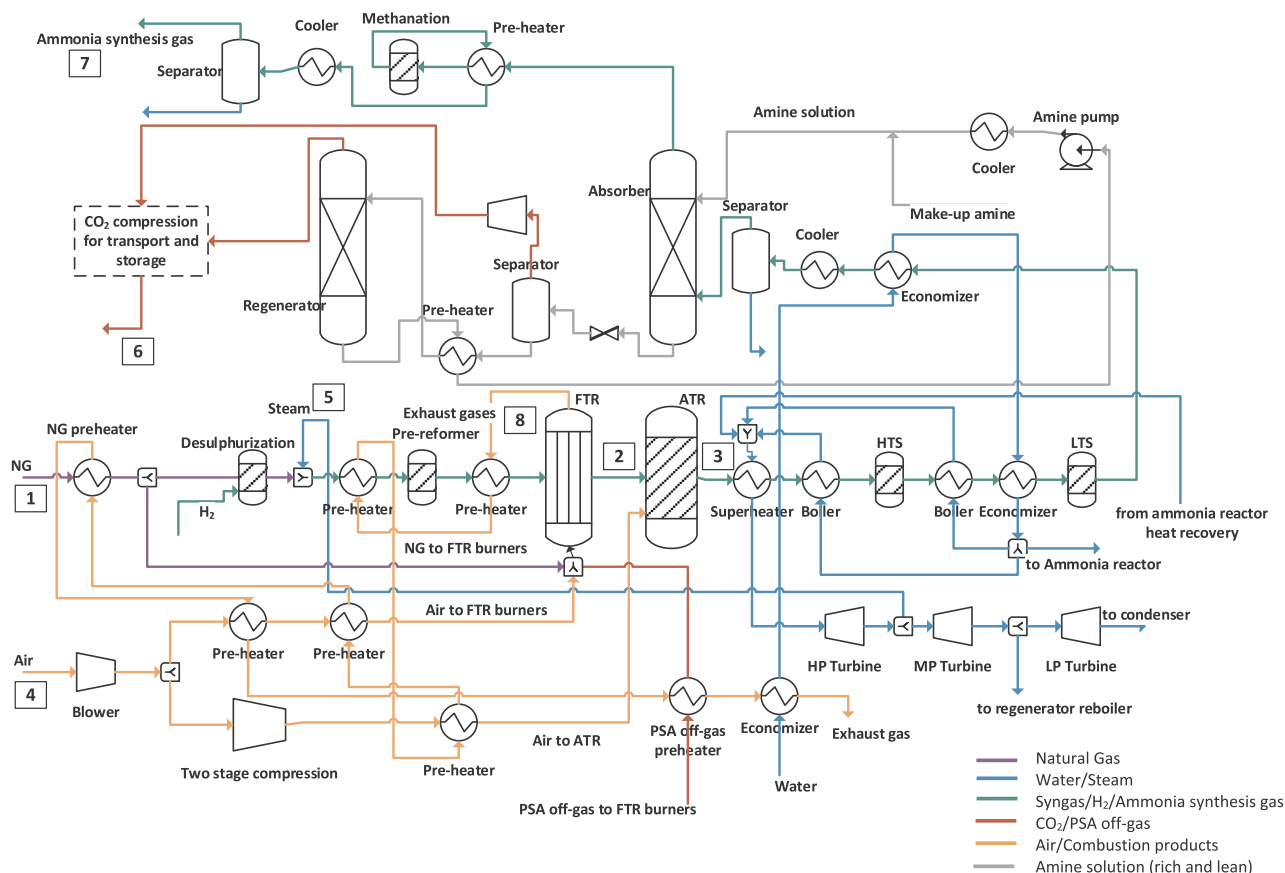

Fig. 5. Schematic of reference ammonia plant (ammonia synthesis loop is shown in Fig. 6).

Table 2
Data from selected streams in Fig. 5 and Fig. 6.

| Stream	T	P	Mass flow	Mole composition (%)									
	°C	bar	kg/s	CH$_4$	C$_{2+}$	N$_2$	O$_2$	CO$_2$	CO	H$_2$O	Ar	H$_2$	NH$_3$
1	15	70.0	10.5	89	8.1	0.89	0.0	2.0	0.0	0.0	0.0	0.0	0.0
2	800	32.4	34.9	7.0	0.0	0.2	0.0	6.3	5.9	40.2	0.0	40.4	0.01
3	996	32.1	54.2	0.2	0.0	15.3	0.0	4.9	9.3	33.0	0.2	37.1	0.04
4	15	1.0	67.8	0.0	0.0	77.3	20.7	0.0	0.0	1.0	0.9	0.0	0.0
5	345	34.4	26.7	0.0	0.0	0.0	0.0	0.0	0.0	1.0	0.0	0.0	0.0
6	25	110.0	20.9	0.0	0.0	0.1	0.0	98.8	0.0	0.2	0.3	0.5	0.0
7	35	25.1	18.3	0.9	0.0	25.0	0.0	0.0	0.0	0.3	0.2	73.7	0.0
8	1067	1.21	51.5	0.0	0.0	71.1	2.6	8.4	0.0	16.9	1.0	0.0	0.0
Ammonia synthesis loop													
9	450	197.0	62.8	8.5	0.0	17.5	0.0	0.0	0.0	0.0	2.1	51.4	20.5
10	26	20.0	17.5	0.6	0.0	0.0	0.0	0.0	0.0	0.2	0.0	0.0	99.2
11	15	1.3	0.7	41.0	0.0	43.0	0.0	0.0	0.0	0.0	5.8	8.8	1.4
12	15	59.4	0.0	0.0	0.0	0.0	0.0	0.0	0.0	0.0	0.0	100.0	0.0

of the amine for CO$_2$ absorption depends on the partial pressure of the CO$_2$ in the feed gas. For moderate partial pressures of CO$_2$ as in this case, which is 5 bar, MDEA is a proposed solution to absorb CO$_2$ [33]. The design conditions in the CO$_2$ absorption and amine regeneration section are similar to the study by Nazir et al. [34]. The CO$_2$ from the regenerator can be compressed for utilization or storage. In this study, the process with and without CO$_2$ capture for utilization/storage is presented.

The synthesis gas from the top of the absorber column contains traces of CO and CO$_2$ that makes the total oxygen content high, which deactivates the ammonia synthesis Fe-based catalyst. Hence, the synthesis gas is pre-heated and sent to the methanation reactor to convert the CO and CO$_2$ into CH$_4$ and H$_2$O over a Ni-based catalyst. The resulting synthesis gas from the methanation reactor is cooled to remove the H$_2$O from the stream, compressed to 199 bar in three stages and sent to the ammonia synthesis reactor (Fig. 6). The ammonia synthesis reaction is highly exothermic and the reactor is operated at 450 °C that results in equilibrium conversion of 20.6%-mol ammonia in the product gas. The product gas from the ammonia synthesis reactor is cooled to 30 °C and is sent to a vapor–liquid separator. The liquid stream is flashed to 20 bar that results in a high purity ammonia stream at the bottom of the flash vessel. The top stream from the flash vessel contains ammonia, hydrogen and methane. This stream is compressed and cooled before being sent to the ammonia scrubber.

The vapor stream from the vapor–liquid separator is passed through a refrigeration loop to recover additional ammonia (81.8% recovery) by condensing it at −20 °C. The refrigeration loop in the ammonia synthesis section uses pure ammonia as the refrigerant that is compressed and expanded between 18 and 1.5 bar pressure. The refrigerant operates between 1 °C and −24.6 °C to condense and recover the ammonia in the stream. The remaining stream contains N$_2$, H$_2$ and NH$_3$. 98.8% of this remaining stream is compressed and re-introduced into the ammonia synthesis reactor, whereas the remainder is sent to the ammonia scrubber. In this way, CH$_4$ and inert gases like Argon are removed to prevent them accumulating in the ammonia synthesis loop. 90% of the ammonia entering the ammonia scrubber is removed, and the remainder of the gas is sent to pressure swing adsorption (PSA) step to recover H$_2$. The recovery of 99.999% pure H$_2$ is calculated using the simplified model specified in Nazir et al. [8]. The off-gas from the PSA is sent to the FTR burners while 87.5% of the recovered H$_2$ is compressed and used in the ammonia synthesis reactor and the remaining 12.5% of the recovered H$_2$ is used in the NG desulphurization section. The ammonia produced from the process is collected in an ammonia tank at 20 bar and 26 °C.

A large amount of heat is recovered within the process while cooling the product streams from ATR, WGS, methanation and ammonia synthesis reactors. In addition, the ammonia synthesis reaction is highly exothermic, and a lot of heat must be extracted to maintain the temperature of the reactor at 450 °C. Heat from these sources is recovered to produce superheated high-pressure (HP) steam at 110 bar and 510 °C. The HP steam is expanded in the steam turbine in three stages. Reforming stream is extracted from the steam turbine at 34.4 bar,
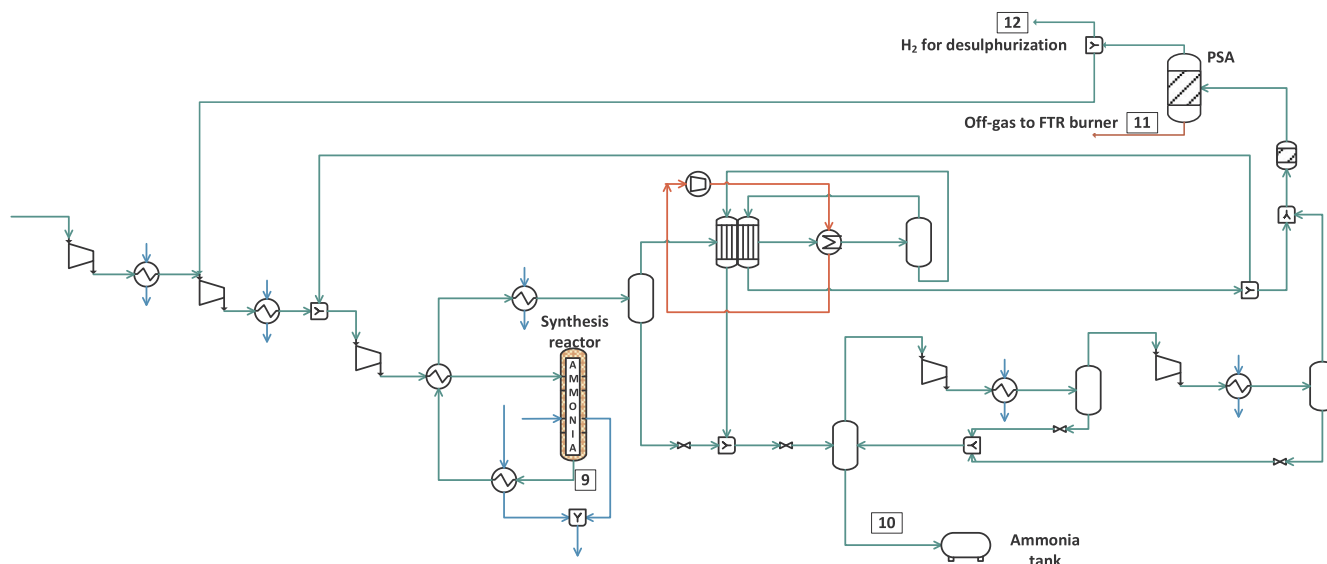
Fig. 6. Schematic of ammonia synthesis loop for the reference plant.

whereas steam for the regenerator boiler in the CO_2 separation section is extracted at 2 bar. The remaining steam is expanded to the condenser pressure of 0.06 bar. Electricity produced from the steam turbine is used to power the compressors and pumps in the process. Excess electricity is sold to the grid. The exhaust gases from FTR contain a lot of heat, which is used to pre-heat the streams in reforming section as well as air and PSA off-gas that is used in the burners. In case of CO_2 compression for transport and storage, the CO_2 stream from the regenerator is compressed to 110 bar in 3 stages [35].

2.2.2. MA-ATR plant

The schematic of the proposed MA-ATR plant for ammonia production is shown in Fig. 7 and Fig. 8 and the stream conditions at key plant locations are listed in Table 3. Large process simplifications are immediately evident when comparing Fig. 7 and Fig. 8 to the reference case in Fig. 5 and Fig. 6. The MA-ATR reactor and ASU displace the functionality of the FTR, ATR, WGS, CO_2 capture and methanation steps. This not only reduces the number of process units, but also greatly simplifies the heat integration scheme.

A conventional double column cryogenic distillation process is adopted for the ASU, delivering oxygen and nitrogen streams at 95% and 99.5% purity, respectively. The airflow rate at the ASU inlet is adjusted in order to produce the required amount of H_2 that in turn produces the same amount of NH_3 as in the reference plant. As a result, there is excess nitrogen available, which is released into the atmosphere. The ASU modelling details along with the schematic are presented in a previous work [16].

Oxygen from the ASU is compressed to 50 bar and fed to the reactor above the membranes to convert any fuel slipping past the membranes. The resulting stream of CO_2 and H_2O is used to preheat the NG and steam to 550 °C at the reactor inlet (stream 4). Upstream, the NG is desulphurized at 300 °C followed by further pre-heating and mixing with process steam at a steam-to-carbon ratio of 1.75. The mixture is pre-reformed at a temperature of 414 °C to convert the higher hydrocarbons before being pre-heated to 550 °C. This stream is reformed to syngas in the MA-ATR reactor where the H_2 permeates through the membranes, favourably shifting the reaction equilibrium towards further hydrogen production.

Nitrogen is compressed to a little over 5 bar and used as the purge stream in the membranes in order to reduce the H_2 partial pressure to enable hydrogen extraction at a higher absolute pressure (lowering compression work before the ammonia loop). The resulting permeate stream is a 3:1 mixture of H_2 and N_2 at a pressure of 5 bar and temperature of 700 °C. A small fraction of O_2 is also present in the N_2 stream and this is assumed to react with the permeated H_2 to form a fraction of H_2O which is small enough to remain in vapour phase until it is condensed out with the produced pure ammonia stream. This high temperature permeate stream is used to preheat the N_2 coming from the ASU to 680 °C before the membrane sweep. The permeate stream is then used to superheat HP steam coming from the NH_3 synthesis reactor (stream 20) and to heat HP water (stream 17) to 290 °C from a temperature of 178 °C after the main economizer in the retentate stream. The HP water stream is then split into two and sent to the NH_3 synthesis reactor for producing superheated high-pressure steam at 110 bar and 430 °C, partly from cooling the outlet stream of the ammonia synthesis reactor (stream 18) and partly from heat removal from within the reactor (stream 19). These streams are mixed and further superheated to 550 °C with the permeate stream as mentioned earlier and expanded to 52.6 bar in the HP steam turbine. Process steam added before the pre-reforming step (stream 21) is split off while the rest is expanded to 3 bar in an intermediate pressure steam turbine and then to 0.03 bar in a low pressure steam turbine, resulting in a vapour fraction above 95% at the turbine outlet. The cooled permeate stream is compressed in five stages to 205 bar to enter the NH_3 loop.

The ammonia synthesis loop is also simplified considerably relative to the reference plant. Since the fraction of impurities (Ar and H_2O) entering the loop is very low, it is possible to remove the refrigeration loop and extract the impurities from the liquid stream after the main flash drum (stream 28). The drawback of not having the refrigeration loop is that no additional ammonia is recovered from the vapour stream from the main flash drum (stream 27). Even though this requires a larger recycle stream, removal of the refrigeration loop remains economically beneficial.

The liquid stream is then throttled to 20 bar to remove additional impurities as vapour (stream 29) to recover ammonia at 99.5% purity (stream 15). The vapour stream is compressed to 56 bar and cooled to
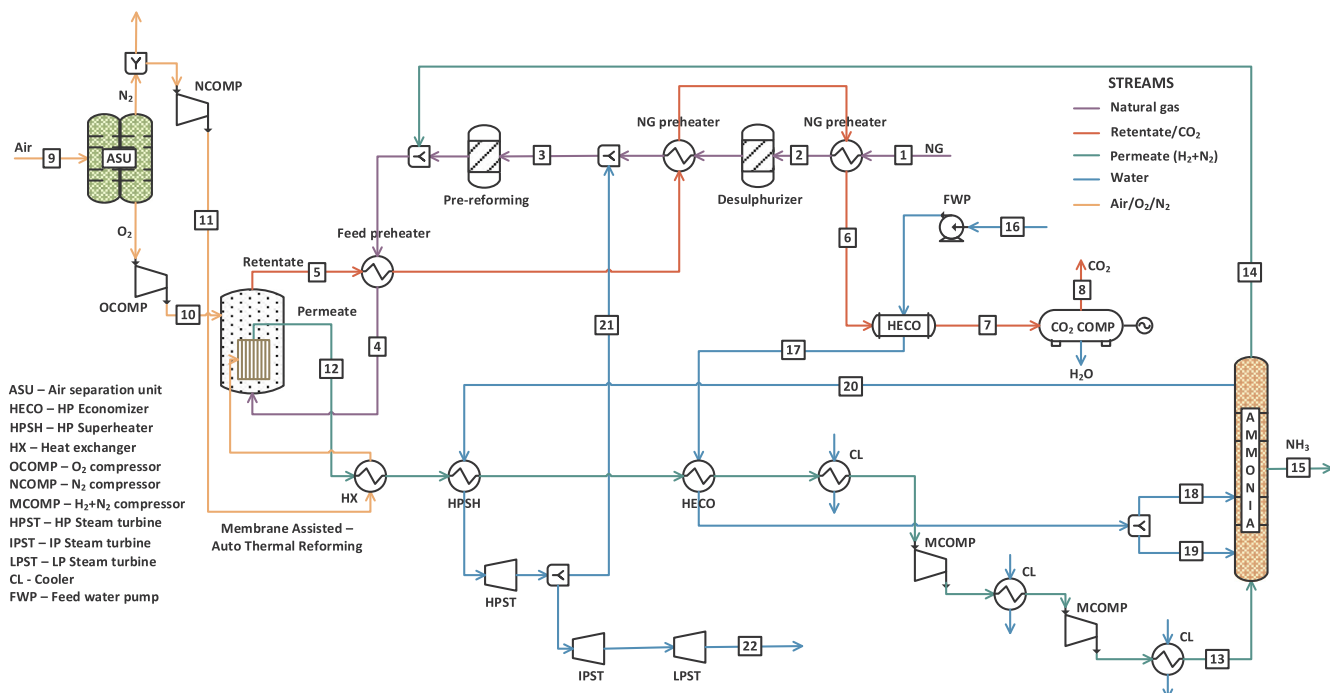

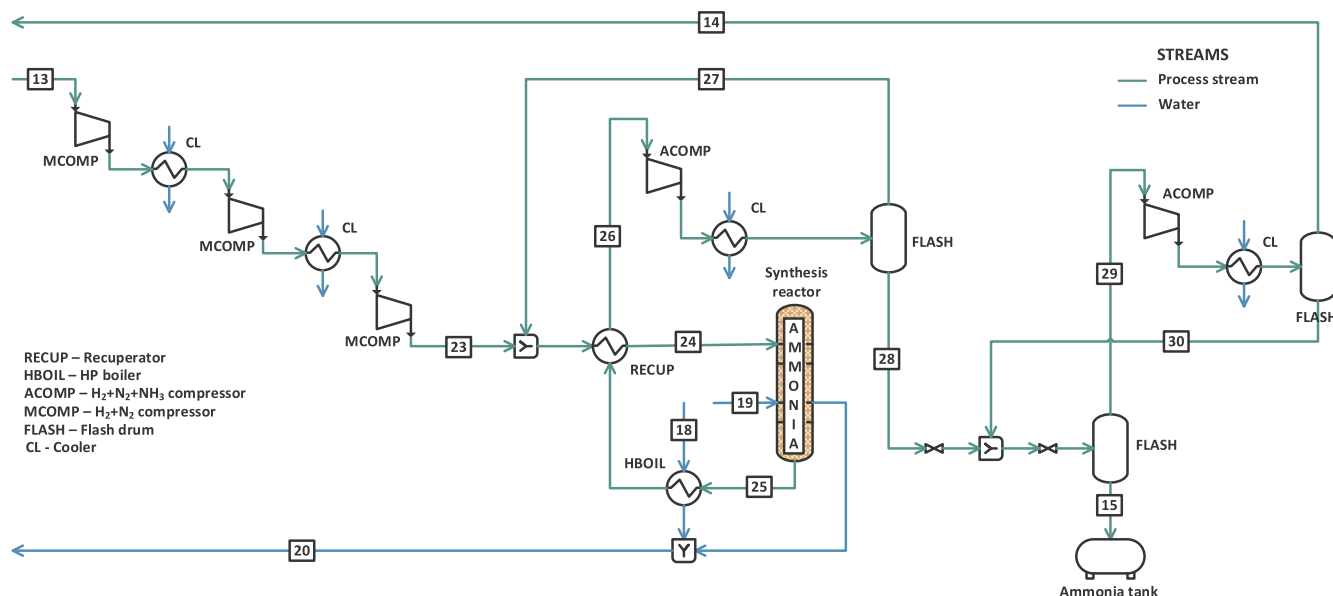**Fig. 7.** Schematic of MA-ATR plant for ammonia production.

Fig. 8. Schematic of ammonia synthesis loop for MA-ATR ammonia plant.

Table 3
Stream conditions at different locations in MA-ATR ammonia plant (Fig. 7 and Fig. 8).

Stream	Temp (°C)	Pressure (bar)	Flow (kg/s)	Species mol fractions									
				N_2	O_2	CO_2	H_2O	AR	CO	H_2	CH_4	C_{2+}	NH_3
1	15.0	70.0	8.4	0.9	0.0	2.0	0.0	0.0	0.0	0.0	89.0	8.1	0.0
2	300.0	68.6	8.4	0.9	0.0	2.0	0.0	0.0	0.0	0.0	89.0	8.1	0.0
3	413.8	52.6	24.2	0.3	0.0	0.7	65.2	0.0	0.0	0.0	31.6	2.2	0.0
4	550.0	51.1	24.4	0.3	0.0	2.2	60.0	0.0	0.0	3.1	34.2	0.0	0.2
5	700.0	49.5	28.2	1.4	0.0	61.6	36.0	1.0	0.0	0.0	0.0	0.0	0.0
6	206.6	46.6	28.2	1.4	0.0	61.6	36.0	1.0	0.0	0.0	0.0	0.0	0.0
7	22.8	45.7	28.2	1.4	0.0	61.6	36.0	1.0	0.0	0.0	0.0	0.0	0.0
8	24.8	110.0	22.8	2.2	0.0	96.2	0.1	1.6	0.0	0.0	0.0	0.0	0.0
9	15.0	1.0	29.0	77.3	20.7	0.0	1.0	0.9	0.0	0.0	0.0	0.0	0.0
10	368.8	50.0	7.0	1.3	95.1	0.0	0.0	3.7	0.0	0.0	0.0	0.0	0.0
11	213.8	5.1	14.4	99.5	0.4	0.0	0.0	0.2	0.0	0.0	0.0	0.0	0.0
12	700.0	5.0	17.5	24.9	0.0	0.0	0.2	0.0	0.0	74.9	0.0	0.0	0.0
13	25.0	21.6	17.5	24.9	0.0	0.0	0.2	0.0	0.0	74.9	0.0	0.0	0.0
14	20.0	56.1	0.2	18.3	0.0	0.0	0.0	2.5	0.0	60.5	0.0	0.0	18.6
15	21.6	20.0	17.4	0.0	0.0	0.0	0.4	0.0	0.0	0.1	0.0	0.0	99.5
16	15.0	1.0	25.2	0.0	0.0	0.0	100.0	0.0	0.0	0.0	0.0	0.0	0.0
17	178.0	115.3	25.2	0.0	0.0	0.0	100.0	0.0	0.0	0.0	0.0	0.0	0.0
18	290.0	114.5	9.7	0.0	0.0	0.0	100.0	0.0	0.0	0.0	0.0	0.0	0.0
19	290.0	114.5	15.4	0.0	0.0	0.0	100.0	0.0	0.0	0.0	0.0	0.0	0.0
20	430.0	112.2	25.2	0.0	0.0	0.0	100.0	0.0	0.0	0.0	0.0	0.0	0.0
21	442.6	52.6	15.8	0.0	0.0	0.0	100.0	0.0	0.0	0.0	0.0	0.0	0.0
22	28.9	0.03	9.4	0.0	0.0	0.0	100.0	0.0	0.0	0.0	0.0	0.0	0.0
23	112.2	205.0	17.5	24.9	0.0	0.0	0.2	0.0	0.0	74.9	0.0	0.0	0.0
24	319.0	200.9	58.5	22.6	0.0	0.0	0.1	0.3	0.0	72.0	0.0	0.0	5.1
25	450.0	198.9	58.5	17.7	0.0	0.0	0.1	0.3	0.0	57.8	0.0	0.0	24.0
26	75.0	191.0	58.5	17.7	0.0	0.0	0.1	0.3	0.0	57.8	0.0	0.0	24.0
27	20.0	206.3	40.9	21.6	0.0	0.0	0.0	0.4	0.0	70.6	0.0	0.0	7.3
28	20.0	206.3	17.6	0.3	0.0	0.0	0.4	0.1	0.0	1.0	0.0	0.0	98.2
29	21.6	20.0	0.3	11.7	0.0	0.0	0.0	1.7	0.0	38.6	0.0	0.0	48.1
30	20.0	56.1	0.2	0.1	0.0	0.0	0.0	0.2	0.0	0.3	0.0	0.0	99.4

recover additional ammonia, with the small stream of remaining impurities (stream 14) sent to the MA-ATR reactor under the assumption that the small fraction of NH_3 (0.2%) will be cracked to N_2 and H_2 in the MA-ATR reactor. If NH_3 is found to cause any problems in the MA-ATR reactor, it could be scrubbed out of the small stream 14 at a minimal cost.

2.3. Economic assessment methodology

2.3.1. Capital costs

Capital costs of the plant were mainly estimated using the methodology and cost functions of Turton et al. [36]. In this methodology, the bare module costs of each individual component of the plant is calculated using the appropriate cost correlation. These costs are then summed up and additional multipliers are added for auxiliaries (50% of bare module cost at standard conditions, i.e. carbon steel and atmospheric pressure) and project contingency (18% of bare module cost) to calculate the total cost of a greenfield plant.

To calculate bare module costs, the equipment purchase cost is first determined based on the size of each component and then increased using multipliers for installation costs as well as the use of more expensive materials and operation at higher pressures. The costs of most

Table 4

Material and pressure assumptions for different plant components.

Process component	Material	Pressure
Heat exchangers	Stainless steel	Depending on process stream
Air compressors	Carbon steel	–
Other compressors	Stainless steel	–
Steam turbines	Stainless steel	–
Flash vessels	Stainless steel clad	Depending on process stream
MA-ATR reactor	Ni-alloy	Atmospheric
MA-ATR shell	Carbon steel	50 bar
NH_3 synthesis reactor	Ni-alloy	Atmospheric
NH_3 synthesis reactor shell	Carbon steel	200 bar

plant components were calculated in this way as detailed in Table 4.

Both the MA-ATR and NH_3 reactors were assumed to consist of two process vessels: an inner vessel made of an expensive Ni-alloy material that carries the temperature and corrosion loads, and an outer vessel made from carbon steel that carries the pressure load. A 20 cm insulation layer is assumed to separate these two layers to ensure that the pressure shell does not weaken from high temperatures. To account for other details of the reactor such as the inlet distributor, the cost of the inner vessel is doubled. This is a crude assumption, but, as will later be shown in the sensitivity assessment, it has almost no effect on the overall economic assessment.

The MA-ATR reactor is sized using the reactor simulation described earlier in this section. The NH_3 synthesis reactor is sized based on the finding of Yancy-Caballero et al. [37] that an inlet flowrate of 7.3 kg/s requires a cross sectional area of 0.78 m^2. The cross-sectional area was scaled linearly with the inlet flowrate from the process simulations in this study and the reactor height was assumed to be 7 m.

Bare module costs of other process components were specified according to the reference costs and capacities identified by Spallina et al. [14] based on other studies [38,39]. Costs of the autothermal reforming reactor were derived from the work of Maqbool and Lee [40] and the cost of the cooling water loop for heat rejection was taken from the EBTF report [41]. Table 5 summarizes the resulting cost data. All costs were adjusted to 2019 prices using the CEPCI index. The resulting bare erected costs were increased by 10% to account for indirect engineering costs [38] to yield the bare module cost. Auxiliary costs were estimated as 25% of the bare module costs for these plant components. This number was selected to result in the same relative cost increase as experienced by all the other plant components (Table 4) evaluated as 50% of bare module costs under standard conditions. Finally, the same 18% project contingency was added.

The cost of the ASU was taken directly from Ebrahimi et al. [42] as 46.3 M$ for a plant producing 6.7 kg/s of O_2. For consistency with the rest of the assessment, this cost was assumed to be composed of 80% bare module costs and 20% auxiliary costs (so that auxiliaries amount to 25% of bare module cost). The 18% contingency was also added on the bare module costs of the ASU. Membrane costs were assumed to be $1000/ft^2 [43]. A 10% membrane installation cost was assumed to find the bare module cost, and the 25% auxiliary and 18% contingency costs

Table 6

Variable operating cost assumptions.

Natural gas price	7 €/GJ [44]
Electricity price	60 €/MWh [44]
Oxygen carrier	15 $/kg [45]
Ni-based catalyst	50 k€/m^3 [14]
Fe-based catalyst	15 k€/m^3 [14]
Cooling water	0.35 €/m^3 [14]
Process water	2 €/m^3 [14]

were added on top.

Finally, another 10% was added to the total greenfield cost to account for interest during plant construction. The resulting total plant cost was then used to calculate annualized capital costs by assuming a 10% discount rate and a 25-year economic lifetime.

2.3.2. Operating costs

Fixed operating costs are assumed to be 5.5% of total greenfield plant costs per year. This consists of 2.5% for operation and maintenance, 2% for insurance and 1% for labour [14].

Important variable operating cost assumptions are summarized in Table 6. Catalyst and oxygen carrier lifetimes were assumed to be 5 years. Membrane lifetimes are assumed to be 2 years with an 80% cost recovery factor upon replacement (assuming that the expensive palladium can be recovered and the membrane support structure can be reused).

2.3.3. Performance measures

Several performance measures are defined to quantify the technical and economic performance of the MA-ATR plant compared to the references. First, the energy intensity and the equivalent energy intensity of NH_3 production [GJ/ton] are defined. The equivalent energy intensity also accounts for the primary energy used to produce the electricity consumed by the plant. In this case, a NGCC plant with an efficiency of 58.3% [41] is assumed, i.e. $\eta_{el} = 0.583$ in Equation (2).

$$\epsilon_{NH_3} = \frac{\dot{m}_{NG} \cdot LHV_{NG}}{\dot{m}_{NH_3}} \tag{1}$$

$$\epsilon_{NH_3,eq} = \frac{\dot{m}_{NG} \cdot LHV_{NG} + \frac{\dot{W}_{el}}{\eta_{el}}}{\dot{m}_{NH_3}} \tag{2}$$

Similarly, the CO_2 emissions intensity and equivalent CO_2 emissions intensity are defined for each plant [ton$_{CO2}$/ton$_{NH3}$]. A natural gas CO_2 intensity of $E_{NG} = 0.057$ ton/GJ is used.

$$e_{NH_3} = \frac{\dot{m}_{NG} \cdot LHV_{NG} \cdot E_{NG}}{\dot{m}_{NH_3}} \tag{3}$$

$$e_{NH_3,eq} = \frac{\left(\dot{m}_{NG} \cdot LHV_{NG} + \frac{\dot{W}_{el}}{\eta_{el}}\right) \cdot E_{NG}}{\dot{m}_{NH_3}} \tag{4}$$

For the economic assessment, the levelized cost of produced NH_3

Table 5

Reference costs, reference capacities, scaling factors and cost years for calculating the bare erected costs of various process components.

Process component	Scaling parameter	Reference capacity	Reference cost (M€)	Scaling factor	Cost year
Desulphurization	Thermal input (MW$_{LHV}$)	413.8	0.66	0.67	2011
Pre-reformer	Thermal input (MW$_{LHV}$)	1800	17.5	0.75	2005
Fired tubular reformer	Thermal input (MW$_{LHV}$)	1246	42.51	0.75	2007
Autothermal reformer	Thermal input (MW$_{LHV}$)	719	6.64	0.75	2013
Water-gas shift	Thermal input (MW$_{LHV}$)	1246	9.54	0.67	2007
Methanation	Thermal input (MW$_{LHV}$)	1246	4.77	0.67	2007
Pressure swing adsorption	Inlet flowrate (kmol/s)	17,069	27.96	0.6	2007
CO_2 capture	CO_2 captured (kg/s)	68.2	46.14	0.8	2011
Heat rejection	Heat rejected (MW)	470	49.6	0.67	2011

[€/ton] is assessed according to Equation (5). Here, C_{cap} (Equation (6)) and $C_{O\&M}$ represent annualized capital and operating costs as outlined in earlier sections [€/year], while the constants, 3.6, 8760 and 0.9 represent the conversion from kg/s to ton/h, the number of hours in a year, and the plant capacity factor, respectively. Finally, the CO_2 avoidance cost is calculated for the MA-ATR and reference plant with CO_2 capture as shown in Equation (7), where the *CCS* and *ref* subscripts denote the plants with and without CO_2 capture respectively.

$$LC_{NH_3} = \frac{C_{cap} + C_{O\&M}}{\dot{m}_{NH_3} \cdot 3.6 \cdot 8760 \cdot 0.9} \tag{5}$$

$$C_{cap} = \frac{c_{cap} d (1 + d)^l}{(1 + d)^l - 1} \tag{6}$$

$$CAC = \frac{LC_{NH_3,CCS} - LC_{NH_3,ref}}{e_{NH_3,ref} - e_{NH_3,CCS}} \tag{7}$$

3. Results and discussion

Results will be presented and discussed in three main sections: technical performance, economic performance and sensitivity analysis.

3.1. Technical performance

The technical performance of the three plants is displayed in Table 7. The first observation is that the MA-ATR plant consumes 20% less fuel than the reference plants for producing the same ammonia output. This is mainly due to the lower operating temperature of the MA-ATR reactor (700 °C) than FTR (1067 °C) and ATR (996 °C) reactors in the reference plant. The MA-ATR plant also avoids heating up a large quantity of air in the FTR furnace. Furthermore, the MA-ATR reactor avoids additional heat production in the WGS and methanation reactors of the reference plant, as well as the heat requirement for regenerating the MDEA solvent. As a result, heat integration is simpler and almost all the energy in the hot MA-ATR outlet streams can be efficiently utilized to pre-heat the inlet streams.

However, since most of the produced heat is effectively fed back into the process, no high-grade heat is available for raising additional steam for power production as in the reference plants. The result is much lower steam turbine power output for the MA-ATR plant. In addition, the mixed H_2 and N_2 stream from the membranes for feeding the NH_3 synthesis loop is produced at a lower pressure (5 bar as opposed to 30 bar), requiring about 12 MW in additional compressor power. Avoidance of the refrigeration loop in the MA-ATR plant saves about 4 MW of compression power, while the ASU, O_2 and N_2 compressors consume about the same power as the air compressors and blowers in the reference plant. The net result is a larger electricity consumption for the MA-ATR plant.

Compressing the captured CO_2 from the reference plant with capture also requires some additional compressor power. The result is that the equivalent energy intensity (Equation (2)) of the MA-ATR plant is 8.4% lower than the reference plant and 10.7% lower than the reference plant with capture. This gain is mainly due to the low efficiency of producing power from steam in the reference plants (~30%) relative to the 58.3% efficiency assumed for the imported electricity from the grid. Thus, if there is a constraint that the plant cannot import efficiently generated grid electricity and must generate all consumed power on-site using a natural gas boiler, the net efficiency advantage of the MA-ATR plant would disappear. Specifically, the equivalent energy intensity of the MA-ATR plant will become equal to the reference plant if the assumed efficiency of imported electricity is reduced to 34%. Clearly, the cost of the imported electricity is important for the MA-ATR plant performance. This will be further explored in the sensitivity analysis.

When looking at emissions, the MA-ATR captures all released CO_2,

whereas the reference plant with capture does not capture the CO_2 produced in the FTR furnace. Even so, the reference plant with capture reduces direct CO_2 emissions by 75% relative to the reference plant without capture. When indirect emissions from consumed electricity are accounted for, the net CO_2 avoidance of the reference plant with capture and the MA-ATR plant becomes 72.2% and 88.7% respectively. The carbon intensity of imported electricity is thus important for the environmental performance of the MA-ATR plant.

3.2. Economic performance

Fig. 9 and Table 8 summarize the results from the economic assessment. Clearly, MA-ATR results in considerably lower levelized costs than both reference plants. This saving is mainly due to lower capital expenditures, which also translate to lower fixed O&M costs. Together, levelized capital and fixed O&M costs of the MA-ATR plant are €31.5/ton NH_3 lower than the reference plant. Variable O&M costs are €4.4/ton higher for MA-ATR than the reference plant because of the added membrane replacement costs. With the assumed natural gas and electricity prices in Table 6, combined fuel and electricity costs for MA-ATR are only €7.9/ton (or 4.0%) lower than that of the reference plant, which is less than would be expected from the 8.4% lower equivalent energy intensity of the MA-ATR plant relative to the reference plant (Table 7). However, fuel and electricity prices vary considerably over time and over different world regions and the effect of variations in these costs will be assessed in the sensitivity analysis.

Thus, the lower capital cost of the MA-ATR plant is the main reason for its superior economic performance with the fuel and electricity prices assumed in the base case. Table 8 indicates that the main process units of the MA-ATR plant (ASU, desulphurization, pre-reformer, MA-ATR reactor, membranes, and NH_3 reactor) are actually more expensive than the more numerous process units of the reference plant (desulphurization, pre-reformer, FTR, ATR, WGS, CO_2 capture, methanation and NH_3 reactor). This is due to the high cost of the ASU and the membranes. The cost of the turbomachinery is also similar, with the reference plant requiring larger turbines to expand the greater quantity of steam produced and the MA-ATR requiring more compressors to compress the H_2 and N_2 stream from the membranes as well as the produced CO_2.

The MA-ATR plant shows considerably lower costs when it comes to pumps, mainly because much less 110 bar steam needs to be raised for heat recovery. In addition, flash vessel costs are lower because of the simplified ammonia loop and avoidance of flash vessels before CO_2 capture, after methanation and within the MDEA process. Another significant saving is in heat rejection because of the higher efficiency of the MA-ATR plant which rejects only 90 MW of heat relative to 157 MW for the reference plant (23% and 32% of NG LHV input for MA-ATR and the reference plant, respectively).

However, the main capital cost advantage of the MA-ATR plant lies

Table 7
Performance of the three plants evaluated in this work.

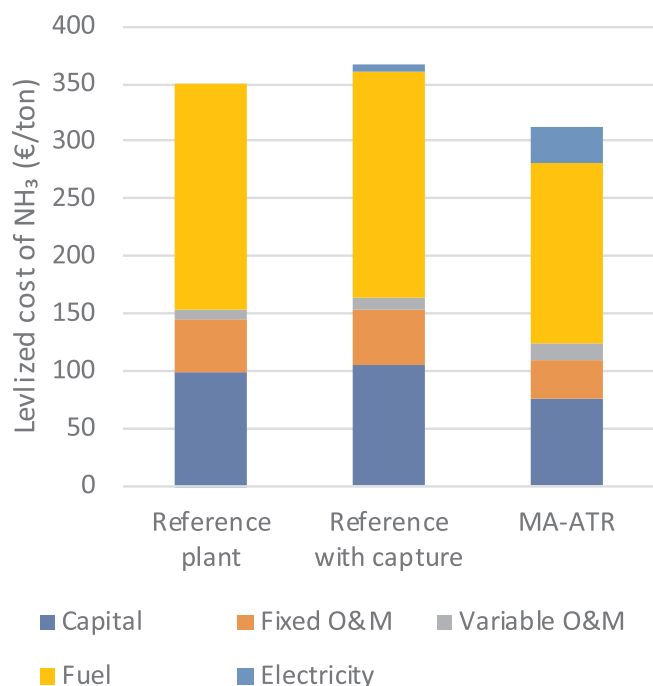|	Reference plant	Reference with capture	MA-ATR
Fuel consumption (MW)	488.7	488.7	390.7
Electricity consumption (MW)	−0.9	6.5	32.0
Turbines	−38.7	−38.7	−12.4
Compressors	35.8	43.0	43.5
Pumps	2.1	2.2	1.0
NH_3 produced (kg/s)	17.3	17.3	17.3
Energy intensity (GJ/ton$_{NH3}$)	28.2	28.2	22.6
Equivalent energy intensity (GJ/ton$_{NH3}$)	28.1	28.9	25.8
CO_2 emissions (ton$_{CO2}$/ton$_{NH3}$)	1.61	0.41	0.00
Equivalent CO_2 emissions (ton$_{CO2}$/ton$_{NH3}$)	1.60	0.45	0.18

Fig. 9. Breakdown of the levelized costs of NH₃ from the three plants evaluated in this work.

Table 8
Economic performance of the three plants evaluated in this work.

	Reference plant	Reference with capture	MA-ATR
Capital costs (M€)			
ir separation unit			30.9
Desulphurization	0.9	0.9	0.7
Pre-reformer	9.5	9.5	8.1
Fired tubular reformer	27.2	27.2	
Autothermal reformer	5.9	5.9	
Water-gas shift	6.6	6.6	
CO_2 capture	20.6	20.6	
Methanation	3.3	3.3	
MA-ATR reactor			12.1
Membranes			27.5
NH₃ reactor	10.4	10.4	9.8
Pressure swing adsorption	2.9	2.9	
Turbines	17.9	17.9	9.5
Compressors	45.5	57.1	56.3
Pumps	12.1	13.6	6.0
Heat exchangers	67.9	70.6	25.8
Flash vessels	14.8	15.3	8.3
Heat rejection	27.5	29.3	19.0
Auxiliaries (M€)	79.8	85.2	53.9
Contingency and fees (M€)	49.2	52.4	38.5
Interest during construction (M€)	40.2	42.9	30.6
Total plant cost (M€)	442.3	471.4	337.1
Annualized costs (M€/year)			
Capital	48.7	51.9	37.1
Operating and insurance	18.1	19.3	13.8
Labour	4.0	4.3	3.1
Catalyst and oxygen carrier	0.7	0.7	0.7
Membrane replacement			2.8
Water	3.7	4.0	3.2
Natural gas	97.1	97.1	77.6
Electricity	− 0.4	3.1	15.2
Levelized cost of NH₃ (€/ton)	349.8	367.0	312.5
CO_2 avoidance cost (€/ton)		14.8	− 24.9

in its simpler heat exchange network with a much lower total heat transfer requirement. Specifically, the total heat transfer duty in the MA-ATR and reference plants are 234 MW and 475 MW, respectively. In addition, all the heat exchangers in the MA-ATR plant operate at high pressures, resulting in relatively high heat transfer coefficients, whereas a considerable number of heat exchangers in the reference plant recover heat from the hot FTR furnace outlet gases close to atmospheric pressure. Thus, the heat exchangers in the MA-ATR plant cost only 38% of those in the reference plant.

Ultimately, the MA-ATR plant achieves a CO_2 avoidance cost of -€24.9/ton, relative to €14.8/ton for the reference plant with capture. This potential to profitably avoid CO_2 (negative CO_2 avoidance cost) offers a promising business case for further scale-up and demonstration of the MA-ATR concept.

When considering the potential of the MA-ATR plant for production of clean ammonia as an energy carrier, it can be noted that the levelized cost of ammonia is €16.8/GJ in LHV terms. This is a large increase relative to the €7/GJ cost of the NG feedstock and a very high CO_2 price of €172/ton would be required for clean ammonia to become competitive with natural gas at these costs. However, ammonia will be more attractive as an international clean energy trade vector where it competes with liquified natural gas (LNG). The 2018 World Energy Outlook [46] gives estimates of the cost of NG liquefaction at about €4.5/GJ. In addition, such plants will be built in regions with cheap NG and electricity. When assuming NG and electricity prices of €3/GJ and €35/MWh, respectively, and adding the €4.5/GJ LNG cost, the required CO_2 price for clean ammonia breakeven with LNG reduces to €65/ton. Ammonia could also bring additional cost savings in terms of transport and storage due to the mild pressures or refrigeration required to maintain a liquid state compared to LNG. A complete lifecycle cost assessment of ammonia relative to LNG will be required for an accurate assessment.

3.3. Sensitivity study

The sensitivity of the economic assessment results to six key parameters is presented in Fig. 10. As could be anticipated from Fig. 9, natural gas price is the most important parameter because it represents 56% of the NH₃ production costs in the reference plant under the base assumptions. Since the MA-ATR plant consumes 20% less natural gas per unit NH₃ produced, it is less sensitive to the natural gas price than the reference plants. Hence, the cost advantage of MA-ATR widens at high natural gas prices and narrows at low natural gas prices.

Since MA-ATR consumes a substantial amount of electricity, it is more sensitive to the electricity price than the reference plants. Thus, Fig. 10b indicates that the cost advantage of MA-ATR widens at low electricity prices and narrows at high electricity prices. However, MA-ATR remains cheaper than the reference case even when electricity prices reach €90/MWh.

Membranes are the most expensive part of the MA-ATR reactor. As Fig. 10c shows, a doubling of membrane prices would erode most of the cost advantage of the MA-ATR process. However, the referenced report [43] for membrane costs targets membrane prices below \$500/ft², implying that it is possible that the MA-ATR cost advantage could increase relative to the base case assumed in this study with continued development and economies of scale related to membrane manufacturing.

Other important membrane-related variables include the permeability, lifetime, cost recovery factor, and maximum operating temperature. The present study assumes an optimistic operating temperature of 700 °C, following Spallina et al. [14], even though the highest temperature for successful long-term tests to date is 650 °C [47,48]. Our previous work showed that reduction of the MA-ATR temperature from 700 °C to 600 °C roughly doubles membrane costs, largely due to SMR equilibrium limitations reducing the hydrogen partial pressure in the reactor [16]. Regarding lifetime and permeability, Arratibel Plazaola
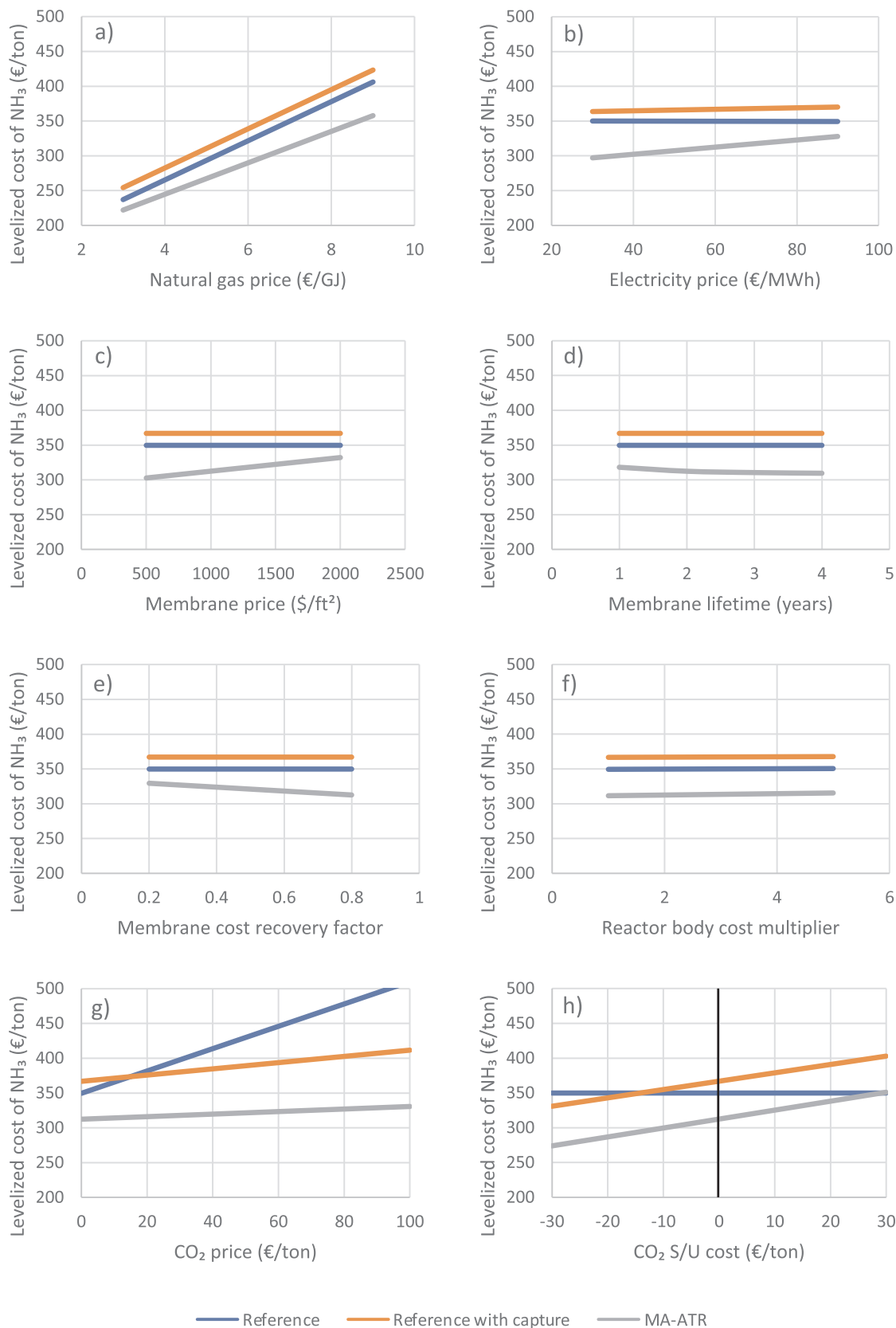
Fig. 10. Sensitivity of the levelized cost of NH₃ to natural gas (a), electricity (b) and membrane (c) prices, membrane lifetime (d) and cost recovery factor (e), reactor costs (f), as well as CO₂ price (g) and storage or utilization (S/U) cost (h). The base levels of the eight parameters are: natural gas price = €7/GJ, electricity price = €60/MWh, membrane price = $1000/ft², membrane lifetime = 2 years, membrane cost recovery factor = 0.8, reactor body cost multiplier = 2, CO₂ price = 0 €/ton, and CO₂ S/U cost = 0 €/ton.

et al. [49] reviewed targets from the United States Department of Energy, stating that a high permeability target of 1.135 mol/m^{2}s with 1.38 bar of H$_2$ partial pressure driving force appears achievable. The hydrogen permeation law applied in the present study returns an H$_2$ flux of only 0.533 mol/m^{2}s with a much higher driving force of about 5 bar, which is well below the targeted membrane permeation performance. Naturally, a doubling of membrane permeability will halve the required membrane surface area and hence also the membrane cost.

The targeted membrane lifetime of 5 years given in Arratibel Plazaola et al. [49] is also well above the assumption of 2 years employed in the present study. However, as shown in Fig. 10d, the membrane lifetime only has a minor effect on the levelized cost of ammonia, mainly due to the high membrane cost recovery factor upon replacement (0.8) assumed. Fig. 10e shows that lower cost recovery factors mildly increase ammonia production costs (e.g., a 5.4% increase if only 20% of membrane costs can be recovered). Overall, the optimistic assumptions regarding operating temperature and membrane cost recovery factor in the present study should be compensated by the conservative membrane permeability and lifetime assumed, creating a reasonable impression of overall economic attractiveness.

Fig. 10f confirms that the uncertain assumption of using a simple multiplier to estimate the costs of the reactor bodies of the MA-ATR and NH$_3$ synthesis reactors relative to the cost of a simple process vessel has almost no effect on the results. Even if the cost of the reactor bodies is 5x higher than the cost of a Ni-alloy process vessel, the relative economic competitiveness of the three plants investigated in this study remains unchanged. Another factor that could affect the MA-ATR reactor cost is the possibility that practical constraints could limit the membrane volume fraction below the value of 0.5 assumed in this study. To investigate this possibility, a new case was completed with a volume fraction of 0.25, which almost doubled the required reactor volume. This case also reduced the required membrane surface area by 13% because the longer gas residence time allowed conversion to approach equilibrium more closely, and the larger reactor diameter allowed for better axial mixing, leading to slightly higher temperatures and higher H$_2$ fractions in the lower regions of the reactor. This reduction in membrane costs combined with the relatively small contribution of the MA-ATR reactor to the total plant cost meant that the ammonia production cost increased by only 0.7% in the case with a membrane volume fraction of 0.25. If membrane costs are kept constant, the cost increase becomes 1.6%.

When looking at CO$_2$ pricing, Fig. 10g shows that the reference plant with CO$_2$ capture becomes more economical than the reference plant without capture at a CO$_2$ price around €15/ton, as suggested by the CO$_2$ avoidance cost in Table 8. The MA-ATR plant extends its advantage over the reference plants at higher CO$_2$ prices due to its high CO$_2$ avoidance. The mild increase in cost of MA-ATR with CO$_2$ price is due to the imported electricity. However, continued increases in CO$_2$ prices will reduce the CO$_2$ intensity of the electricity supply, reducing this effect.

Finally, CO$_2$ storage or utilization (S/U) costs are shown to have a significant effect on the two plants with CO$_2$ capture (Fig. 10h). Negative costs of CO$_2$ S/U (i.e., profitable CO$_2$ utilization) is possible when ammonia is used for urea production. Given the portability of ammonia, it is also possible that future ammonia energy carrier production plants can be situated close to oil and gas operations to enable easy access to profitable enhanced oil recovery opportunities, which can be worth about €30/ton of CO$_2$ avoided [50]. On the other end of the spectrum, a high CO$_2$ S/U cost of €30/ton erodes the cost advantage of MA-ATR over the reference plant.

In general, this sensitivity analysis shows that the conclusion that MA-ATR can produce clean ammonia at considerably lower costs than benchmark plants is robust.

4. Summary and conclusions

The present study presented a techno-economic assessment of a new configuration for ammonia production from natural gas based on the membrane-assisted autothermal reforming (MA-ATR) reactor. This technology can displace the fired tubular reformer, autothermal reformer, water gas shift (WGS) reactors, CO$_2$ capture plant, methanation reactor and pressure swing adsorption unit in a conventional NH$_3$ plant with a single MA-ATR reactor and a conventional air separation unit (ASU). In addition, MA-ATR produces a high-purity H$_2$ and N$_2$ mixture, allowing for significant additional simplifications to the ammonia production loop.

Aside from the substantial process intensification benefits, MA-ATR also offers significant efficiency improvements. It operates at much lower temperatures than FTR and ATR and avoids separate exothermic reactions in the WGS and methanation reactors. Therefore, it produces much less heat, reducing natural gas consumption by 20% relative to the reference plant. However, MA-ATR needs to import a substantial amount of electricity, which reduces its overall efficiency benefit to 8.4%.

From an economic point of view, there are no direct benefits from the reduction in the number of process units because of the high cost of the membranes and the ASU. However, substantial capital cost reductions are achieved mainly from the much simpler heat exchange network. Because MA-ATR produces much less heat than the reference plant, the total amount of heat exchange duty required is less than half that of the reference plant. In combination with the efficiency gains, this makes NH$_3$ production from MA-ATR 10.7% cheaper than the reference plant without CO$_2$ capture and 14.9% cheaper than the reference plant with CO$_2$ capture. This competitive advantage would improve with higher natural gas prices, lower electricity prices, lower membrane costs and higher CO$_2$ prices.

In terms of CO$_2$ avoidance, MA-ATR has no direct CO$_2$ emissions, but indirect emissions from imported electricity must be accounted for. If imported electricity comes from a natural gas combined cycle power plant, the net CO$_2$ avoidance of MA-ATR is 88.7% relative to 72.2% for the reference plant with CO$_2$ capture. CO$_2$ avoidance costs amount to −24.9 and 14.8 €/ton for the MA-ATR and reference plant with CO$_2$ capture, respectively.

The considerable cost reduction achieved by MA-ATR relative to benchmarks improves the feasibility of using ammonia as a clean energy carrier in the future. A simple estimate revealed that CO$_2$ prices of around €65/ton would be required for clean ammonia from MA-ATR to compete with LNG for energy export from large natural gas producing regions. A complete lifecycle cost assessment of ammonia and LNG is required to draw more accurate conclusions in this respect.

Finally, it can be noted that all process components in the proposed MA-ATR ammonia plant are mature technologies, aside from the membranes and the oxygen carrier. To capitalize on the promising techno-economic performance revealed in this study, further studies focussed on the development and eventual commercialization of these two elements are recommended.

Declaration of Competing Interest

The authors declare that they have no known competing financial interests or personal relationships that could have appeared to influence the work reported in this paper.

Acknowledgement

authorities: the Research Council of Norway and the European Commission.

References

[1] IPCC, Global Warming of 1.5 °C, Intergovernmental Panel on Climate Change, 2018.

[2] IEA, The future of hydrogen: Seizing today's opportunities, International Energy Agency (2019).

[3] M. Rydén, A. Lyngfelt, T. Mattisson, Synthesis gas generation by chemical-looping reforming in a continuously operating laboratory reactor, Fuel 85 (2006) 1631–1641.

[4] M. Ryden, A. Lyngfelt, T. Mattisson, Two novel approaches for hydrogen production; chemical-looping reforming and steam reforming with carbon dioxide capture by chemical-looping combustion, 16th World Hydrogen Energy Conference 2006, WHEC 2006, June 13, 2006 – June 16, 2006, Association Francaise pour l'Hydrogene et les Piles a, Lyon, France, 2006, pp. 703-710.

[5] M. Ishida, D. Zheng, T. Akehata, Evaluation of a chemical-looping-combustion power-generation system by graphic exergy analysis, Energy 12 (1987) 147–154.

[6] A. Lyngfelt, B. Leckner, T. Mattisson, A fluidized-bed combustion process with inherent CO2 separation; Application of chemical-looping combustion, Chem. Eng. Sci. 56 (2001) 3101–3113.

[7] S.A. Wassie, J.A. Medrano, A. Zaabout, S. Cloete, J. Melendez, D.A.P. Tanaka, S. Amini, M. van Sint Annaland, F. Gallucci, Hydrogen production with integrated CO2 capture in a membrane assisted gas switching reforming reactor: proof-of-Concept, Int. J. Hydrogen Energy 43 (2018) 6177–6190.

[8] S.M. Nazir, J.H. Cloete, S. Cloete, S. Amini, Efficient hydrogen production with CO2 capture using gas switching reforming, Energy 185 (2019) 372–385.

[9] S.M. Nazir, J.H. Cloete, S. Cloete, S. Amini, Pathways to low-cost clean hydrogen production with gas switching reforming, Int. J. Hydrogen Energy (2020).

[10] V. Spallina, G. Motamedi, F. Gallucci, M. van Sint Annaland, Techno-economic assessment of an integrated high pressure chemical-looping process with packed-bed reactors in large scale hydrogen and methanol production, Int. J. Greenhouse Gas Control 88 (2019) 71–84.

[11] P. Chiesa, G. Lozza, A. Malandrino, M. Romano, V. Piccolo, Three-reactors chemical looping process for hydrogen production, Int. J. Hydrogen Energy 33 (2008) 2233–2245.

[12] V. Hacker, R. Fankhauser, G. Faleschini, H. Fuchs, K. Friedrich, M. Muhr, K. Kordesch, Hydrogen production by steam–iron process, J. Power Sources 86 (2000) 531–535.

[13] D.-A. Chisalita, C.-C. Cormos, Techno-economic assessment of hydrogen production processes based on various natural gas chemical looping systems with carbon capture, Energy 181 (2019) 331–344.

[14] V. Spallina, D. Pandolfo, A. Battistella, M.C. Romano, M. Van Sint Annaland, F. Gallucci, Techno-economic assessment of membrane assisted fluidized bed reactors for pure H2 production with CO2 capture, Energy Convers. Manage. 120 (2016) 257–273.

[15] J.A. Medrano, I. Potdar, J. Melendez, V. Spallina, D.A. Pacheco-Tanaka, M. van Sint Annaland, F. Gallucci, The membrane-assisted chemical looping reforming concept for efficient H2 production with inherent CO2 capture: experimental demonstration and model validation, Appl. Energy 215 (2018) 75–86.

[16] S. Cloete, M.N. Khan, S. Amini, Economic assessment of membrane-assisted autothermal reforming for cost effective hydrogen production with CO2 capture, Int. J. Hydrogen Energy 44 (2019) 3492–3510.

[17] A. Valera-Medina, H. Xiao, M. Owen-Jones, W.I.F. David, P.J. Bowen, Ammonia for power, Prog. Energy Combust. Sci. 69 (2018) 63–102.

[18] M. Niermann, S. Drünert, M. Kaltschmitt, K. Bonhoff, Liquid organic hydrogen carriers (LOHCs) – techno-economic analysis of LOHCs in a defined process chain, Energy Environ. Sci. 12 (2019) 290–307.

[19] S. Giddey, S.P.S. Badwal, A. Kulkarni, Review of electrochemical ammonia production technologies and materials, Int. J. Hydrogen Energy 38 (2013) 14576–14594.

[20] P. Peng, P. Chen, C. Schiappacasse, N. Zhou, E. Anderson, D. Chen, J. Liu, Y. Cheng, R. Hatzenbeller, M. Addy, Y. Zhang, Y. Liu, R. Ruan, A review on the non-thermal plasma-assisted ammonia synthesis technologies, J. Cleaner Prod. 177 (2018) 597–609.

[21] I. Martínez, D. Armaroli, M. Gazzani, M.C. Romano, Integration of the Ca-Cu process in ammonia production plants, Ind. Eng. Chem. Res. 56 (2017) 2526–2539.

[22] J. Andersson, J. Lundgren, Techno-economic analysis of ammonia production via integrated biomass gasification, Appl. Energy 130 (2014) 484–490.

[23] J. Xu, G.F. Froment, Methane steam reforming, methanation and water-gas shift: I. Intrinsic kinetics, AIChE J. 35 (1989) 88–96.

[24] E.L.G. Oliveira, C.A. Grande, A.E. Rodrigues, Methane steam reforming in large pore catalyst, Chem. Eng. Sci. 65 (2010) 1539–1550.

[25] A. Abad, J. Adánez, F. García-Labiano, L.F. de Diego, P. Gayán, J. Celaya, Mapping of the range of operational conditions for Cu-, Fe-, and Ni-based oxygen carriers in chemical-looping combustion, Chem. Eng. Sci. 62 (2007) 533–549.

[26] E. Fernandez, J.A. Medrano, J. Melendez, M. Parco, J.L. Viviente, M. van Sint Annaland, F. Gallucci, D.A. Pacheco Tanaka, Preparation and characterization of metallic supported thin Pd–Ag membranes for hydrogen separation, Chem. Eng. J. 305 (2016) 182–190.

[27] G.S. Lee, S.D. Kim, Axial mixing of solids in turbulent fluidized beds, Chem. Eng. J. 44 (1990) 1–9.

[28] Y. Igci, A.T. Andrews, S. Sundaresan, S. Pannala, T. O'Brien, Filtered two-fluid models for fluidized gas-particle suspensions, AIChE J. 54 (2008) 1431–1448.

[29] W. Holloway, S. Sundaresan, Filtered models for reacting gas–particle flows, Chem. Eng. Sci. 82 (2012) 132–143.

[30] S.A. Wassie, S. Cloete, V. Spallina, F. Gallucci, S. Amini, M. van Sint Annaland, Techno-economic assessment of membrane-assisted gas switching reforming for pure H2 production with CO2 capture, Int. J. Greenhouse Gas Control 72 (2018) 163–174.

[31] N. Masoumifard, N. Mostoufi, A.-A. Hamidi, R. Sotudeh-Gharebagh, Investigation of heat transfer between a horizontal tube and gas–solid fluidized bed, Int. J. Heat Fluid Flow 29 (2008) 1504–1511.

[32] AspenHYSYS, Aspen HYSYS V8.6 User Guide, Aspen Technology Inc., Bedford, Massachusetts, USA, 2017.

[33] M. Appl, Ammonia: Principles and Industrial Practice, (1999).

[34] S.M. Nazir, J.F. Morgado, O. Bolland, R. Quinta-Ferreira, S. Amini, Techno-economic assessment of chemical looping reforming of natural gas for hydrogen production and power generation with integrated CO2 capture, Int. J. Greenhouse Gas Control 78 (2018) 7–20.

[35] EBTF, European best practice guidelines for assessment of CO2 capture technologies. CESAR -project 7th FrameWork Programme. Collaborative Project– GA No. 213569, 2011.

[36] R. Turton, R.C. Bailie, W.B. Whiting, J.A. Shaeiwitz, Analysis, Synthesis and Design of Chemical Processes: Appendix A, Pearson Education, 2008.

[37] D. Yancy-Caballero, L. Biegler, R. Guirardello, Optimization of an ammonia synthesis reactor using simultaneous approach, Chem. Eng. Trans. 43 (2015) 1297–1302.

[38] NETL, Assessment of hydrogen production with CO2 capture, Volume 1: Baseline state-of-the-art plants, National Energy Technology Laboratory, 2010.

[39] G. Manzolini, E. Macchi, M. Gazzani, CO2 capture in Integrated Gasification Combined Cycle with SEWGS – Part B: Economic assessment, Fuel 105 (2013) 220–227.

[40] W. Maqbool, E.S. Lee, Syngas Production Process Development and Economic Evaluation for Gas-to-Liquid Applications, 37 (2014) 995-1001.

[41] EBTF, European best practice guide for assessment of CO2 capture technologies, European Benchmark Task Force, 2011.

[42] A. Ebrahimi, M. Meratizaman, H. Akbarpour Reyhani, O. Pourali, M. Amidpour, Energetic, exergetic and economic assessment of oxygen production from two columns cryogenic air separation unit, Energy 90 (2015) 1298–1316.

[43] J. Acquaviva, High-Performance, Durable, Palladium Alloy Membrane for Hydrogen Separation and Purification, Pall Corporation, 2009.

[44] CREG, A European comparison of electricity and gas prices for large industrial consumers, PwC Enterprise Advisory, 2018.

[45] J. Adanez, A. Abad, F. Garcia-Labiano, P. Gayan, L.F. de Diego, Progress in Chemical-Looping Combustion and Reforming technologies, Prog. Energy Combust. Sci. 38 (2012) 215–282.

[46] IEA, World Energy Outlook, International Energy Agency, 2018.

[47] J. Okazaki, T. Ikeda, D.A. Pacheco Tanaka, M.A. Llosa Tanco, Y. Wakui, K. Sato, F. Mizukami, T.M. Suzuki, Importance of the support material in thin palladium composite membranes for steady hydrogen permeation at elevated temperatures, Phys. Chem. Chem. Phys. 11 (2009) 8632–8638.

[48] H. Jia, P. Wu, G. Zeng, E. Salas-Colera, A. Serrano, G.R. Castro, H. Xu, C. Sun, A. Goldbach, High-temperature stability of Pd alloy membranes containing Cu and Au, J. Membr. Sci. 544 (2017) 151–160.

[49] A. Arratibel Plazaola, D.A. Pacheco Tanaka, M. Van Sint Annaland, F. Gallucci, Recent advances in Pd-based membranes for membrane reactors, Molecules (Basel, Switzerland) 22 (2017) 51.

[50] S. Roussanaly, A.-A. Grimstad, The economic value of CO2 for EOR applications, Energy Procedia 63 (2014) 7836–7843.